A study of gas-stopping of intense energetic rare isotope beams

G. Bollen[a,b,*], D.J. Morrissey[a,c], S. Schwarz[a]

[a]*National Superconducting Cyclotron Laboratory, Michigan State University, East Lansing, MI 48824, USA*
[b]*Department of Physics and Astronomy, Michigan State University, East Lansing, MI 48824, USA*
[c]*Department of Chemistry, Michigan State University, East Lansing, MI 48824, USA*

Abstract

A scheme is proposed for the efficient thermalization of energetic and intense rare isotope beams. Simulation results indicate that gas stopping of heavy ions in a weakly focusing magnetic field can overcome the severe intensity limitation that exists in present systems and also provide a much faster ion extraction.
© 2005 Elsevier B.V. All rights reserved.

1. Introduction

At present, several groups around the world are working on projects to stop fast ion beams in gas catchers [1–4]. The conversion of relativistic fragments into low-energy exotic beams with a gas stopper is a challenging task. It is considered important because it has the potential to connect rare isotope beam production via projectile fragmentation to ISOL-type experimental techniques. With a number of refractory-element beams not

available at ISOL facilities and advantages in the production of the most exotic nuclides, a wealth of new experiments with stopped and post-accelerated ion beams could become possible. The gas-stopping scenario is integral part of the concept for the proposed Rare Isotope Accelerator Facility [5,6].

The present gas catcher systems [1–4] are all based on the slowing down of fast beams in solid degraders and their final stopping in a gas-filled chamber. This stopping cell is equipped with electrodes that allow the stopped ions to be transported to a small orifice by means of static and/or radiofrequency (RF) electric fields. Assisted by gas flow the ions are swept out of the gas cell through this orifice and then guided with RF

---

*Corresponding author. National Superconducting Cyclotron Laboratory, Michigan State University, East Lansing, MI 48824, USA. Tel.: +1 517 333 6435; fax: +1 517 353 5967.

E-mail address: bollen@nscl.msu.edu (G. Bollen).

techniques through a series of differential pumping stages before they are accelerated to the desired beam energy. For the stopping of fragmentation beams with large momentum distributions an ion-optical compression [7–9] of the beam momentum distribution is a must in order to keep the gas cell size reasonable and to minimize ion extraction times.

The NSCL gas stopping system has seen most of the experimental tests of stopping fast beams with energies of about 100 MeV/u [1]. A large number of studies of stopping and extracting energetic fragments from the NSCL gas cell have been completed and the results have been published [10–12]. A stopping efficiency of the order of 50% for beams with narrow momentum distributions has been achieved and extraction efficiencies as high as 8% have been observed for beam rates below 100/s [1]. A decrease in efficiency by a factor of 4 was observed for rates larger than 10^4/s. This observation of a rate dependent efficiency is in agreement with observations made with a related gas cell system at RIKEN [4,13]. The reduction in efficiency is attributed to the buildup of space charge due to the ionization process. Recent particle-in-cell (PIC) simulations confirmed quantitatively the experimental findings at the NSCL [14].

It appears that without a major change in concept, gas stopping of fast beams may not be applicable to beam intensities much larger than 10^6/s without a major loss of efficiency. Hence, the usefulness of the present approaches for next-generation high-power rare isotope beam facilities has to be questioned. Another shortcoming of present gas stopper concepts is the rather large extraction time for the stopped ions. The average extraction time is in the order of several tens of milliseconds and those ions stopped farthest from the orifice often need more than 100 ms to be extracted. This means that the present schemes introduce significant decay losses for very short-lived isotopes. This is highly undesirable in order to make best use of the practically decay-loss-free fast-beam production. Ideally, extraction times should be on the order of a few milliseconds, which is the range of the shortest beta-decay half-lives observed so far.

In the following we propose and investigate a concept in which space charge effects are reduced and as a consequence the intensity limits are significantly increased. At the same time the concept promises much faster ion extraction than conventional gas stopper systems.

2. Proposed concept

In order to reduce the effects of space charge in gas stoppers and to decrease ion extraction times we investigate a scheme, in which ions are slowed down by gas collisions inside the field of a weakly focusing cyclotron-type magnet. The focusing properties of the magnet allow the ions to be confined in all dimensions during the slowing down process and they can be stopped along a much longer path in lower pressure compared to "conventional" gas stoppers used for this purpose. Such a cyclotron stopper scheme is not completely new. It has been successfully used for the stopping of antiprotons, pions and muons [15,16] for the production and subsequent studies of exotic atoms. The scheme has also been proposed by Katayama et al. [17] to be used for the stopping of light ions. They recognized that such a "cyclotron ion guide" would allow ions to be stopped at low pressure and provide fast ion extraction. They theoretically investigated the properties of an RF carpet, originally discussed by Masuda [18], and its ability to transport the ions loss-free to an extraction system. We have extended this work by studying the application of such a scheme to the stopping of heavy ion beams of high intensity and the accompanying effects of ionization and space charge.

Fig. 1 shows a schematic overview of the proposed concept for such an ion beam stopper. It consists of a weak focusing cyclotron magnet and a gas-filled vacuum chamber with charge collection electrodes. The transport of the ions to an extraction orifice uses an RF carpet. An RFQ ion guide transports the ions through a differential pumping system out of the magnet. The possibility to install a test ion source is also indicated.
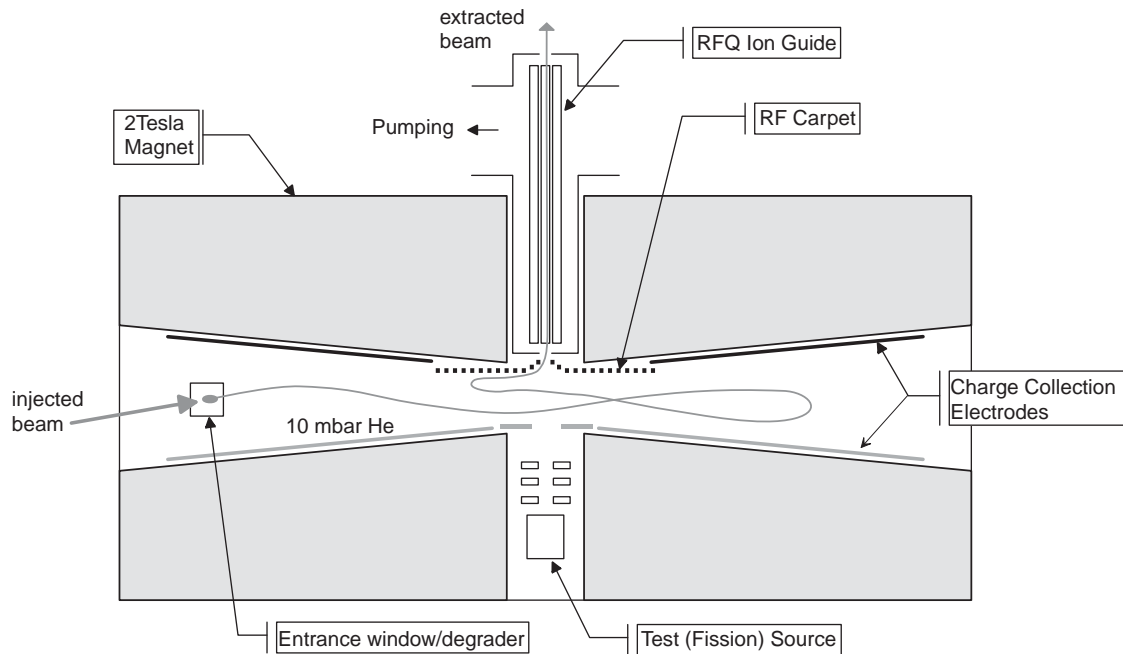
Fig. 1. Improved concept for the stopping of fast heavy ion beams and their conversion into low-energy ion beams. The sketch shows the main components of the system which are a weakly focusing magnet system containing the vacuum chamber filled with 10 mbar of He, charge collection liners, a RF funnel for ion extraction and a differentially pumped RFQ ion guide system. The position for the possible installation of a test beam ion source is also indicated.

Expected features of this gas-stopping concept for intense and energetic heavy ion beams are:

- The 'infinite' length of the stopping path allows a low gas pressure to be used.
- The large stopping volume and low gas pressure reduce space charge effects caused by the ionization of the helium atoms.
- The volume in which the stopping process takes place is expected to have a disk-like shape; electric fields in the direction of the magnetic field should efficiently remove helium ions and electrons during the slowing down process and help to further reduce space charge effects.
- The ions stop in a small central region of the system.
- The low gas pressure is of advantage for employing radiofrequency techniques for the ion extraction.

In order to assess the practicality of such a scheme we simulated the stopping of heavy ions in such a

system. We also investigated the theoretical effect of strong magnetic fields on the performance of RF carpets and ion guides, needed for the collection and extraction of the ions once they are stopped.

3. Simulations

3.1. Stopping calculations

A dedicated Monte Carlo beam tracing code was written to study ion stopping in the system sketched in Fig. 1. Ions thought to have already passed a solid energy degrader are injected tangentially to a circle with radius r_{inj}, centered at the symmetry axis of the magnetic field. The ions' motion is calculated taking the Lorentz force and energy dependent stopping power into account as well as charge exchange. The latter is necessary to correctly describe the motion of the ions in the magnetic field. As a test case for our

simulations we chose bromine, because it is a medium heavy nucleus and since charge exchange data are available for this element. A 100 MeV/u beam was assumed to pass through a 2.62 mm thick Al degrader. An average energy of 610 MeV (8 MeV/u) after degrading was determined with SRIM [19] and used as the initial mean beam energy. Other parameters used for the simulation are listed in Table 1.

3.1.1. Basis for simulations

Since the ion energy after retardation corresponds to an ion velocity $v < 0.1c$, the motion of the ion was treated non-relativistically. An axial-symmetric magnetic field $\vec{B}(\vec{\rho}, z) = B_\rho \cdot \hat{\rho} + B_z \cdot \hat{z}$ was assumed. In paraxial approximation this field can be described by

$$B_\rho = -(n_0 \cdot B_0 / r_{inj}) z \tag{1}$$

$$B_z = B_0 - (n_0 \cdot B_0 / r_{inj}) \rho \tag{2}$$

where n_0 denotes the field index at the radius r_{inj} of beam injection and B_0 the maximum field strength. Besides the Lorentz force, the stopping force appears in the equation of motion

$$m\ddot{\vec{r}} = q(v) \cdot \vec{v} \times \vec{B} - S(v) \cdot \frac{\vec{v}}{v}. \tag{3}$$

The stopping power $S(v)$ was obtained from SRIM stopping tables for bromine ions in helium and parameterized for energies from 1 GeV down to 100 eV. Small angle scattering and energy straggling are not considered in the code, since these effects are relatively small for ion stopping in helium and are small compared to the initial beam parameters. Multiple-electron loss or capture have

Table 1
Parameters used in the simulations

Magnetic field strength B	2 T
Field index n_0 at r_{inj}	0.2
Helium pressure p_{He}	10 mbar
Ion species	^{78}Br
Ion kinetic energy E	610 MeV
Relative energy spread (full width) $\Delta E/E$	20%
Injection radius r_{inj}	0.8 m
Beam half width $w/2$	5 mm
Beam half divergence $\theta/2$	10 mrad

also been neglected since the cross-sections are more than an order of magnitude smaller than those for one-electron processes.

The change of the charge state $q(v)$ during the stopping process is considered in some detail in this code. The cross-sections for electron capture and loss and the average charge state $\bar{q}$ depend strongly on the ion velocity and the atomic number of the ion. Experimental cross-sections are only known for a very limited number of elements and energies. In order to determine the charge exchange cross-sections we used formulae and data summarized in a review article by Betz [20]. The cross-sections for electron capture σ_c and loss σ_1 are assumed to follow exponential functions:

$$\sigma_c = \frac{\sigma_0}{2} \cdot e^{a_c(q - \bar{q})} \tag{4}$$

$$\sigma_1 = \frac{\sigma_0}{2} \cdot e^{a_1(\bar{q} - q)} \tag{5}$$

where $\bar{q}$ is the average charge state for a given velocity and q is the actual charge state of the ions. The average charge state $\bar{q}$ of the ion as a function of its velocity v is determined by semi-empirical formulae (Eqs. (5.4) and (5.5) in Ref. [20]) with parameters fitted to experimental data. These formulae reproduce experimental data on a better than 10-percent level up to 200 MeV.

Data listed in Ref. [20] for bromine ions at energies of 6, 10 and 14 MeV have been used together with Eqs. (4) and (5) to parameterize a_c, a_1 and σ_0 and their energy dependence. The values for a_c and a_1 determine the width and shape of the equilibrium charge state distribution, which is not very critical for the simulations performed here. Their energy dependence has been parameterized for lower energies and they are kept identical and constant for energies higher than 14 MeV. A realistic function for the cross-section σ_0 is important since σ_0 determines the mean free path λ of the ions between charge exchanges. If λ is a large fraction of the circumference of the approximately circular motion, large beam deflections will occur when the ions change charge states. In addition to using the low energy data σ_0 has also been parameterized to match the value for 600 MeV, calculated by using Eq. (4.7) in Ref. [20],

a formula originally derived by Bohr for charge-changing of heavy ions in light targets.

The total cross-section $\sigma = \sigma_c + \sigma_l$ is used to determine the mean free path $\lambda = 1/(n \cdot \sigma)$ and the period $\tau = \lambda/v$ of the ions between two charge exchange reactions. Here, n is the atom density of the stopping gas and v the ion velocity. During this period the ions are assumed to move with one charge state in the magnetic field while simultaneously losing energy as given by the stopping power S. At a vertex, the charge state of an ion is changed randomly according to the probability to lose or capture an electron as given by the cross-sections σ_c and σ_l. For an injection energy of 610 MeV and a helium pressure of $p_{He} = 10$ mbar the mean free path λ is about 6 mm and more than two orders of magnitude smaller when the ions come to rest. This means all ions will follow very closely a trajectory given by the equilibrium charge state.

The trajectory calculation is terminated once an ion has reached an energy of 100 eV or less. Data files are created with information on the final ion distribution and on the energy deposition in the radial plane. Data files are also created for a set of complete trajectories together with information on charge states, time-of-flight and path length.

3.1.2. Simulation results

Fig. 2 shows the three-dimensional trajectory and projections of a single 610 MeV ^{78}Br ion in a magnetic field of $B = 2$ T with a field index of $n_0 = 0.2$ at $r_{inj} = 0.8$ m. It can be seen that the ion moves within a disk-like volume. Fig. 3 shows the trajectories for a number of ions representative of an injected beam with the parameters in Table 1. After one turn the ions are well separated from the injected beam, which is important to avoid beam losses. All ion trajectories end in the central region of the system. Fig. 4 shows the axial motion of two ions starting with $z = w$ and elevation angles $\pm\theta/2$ (see Table 1) as a function of time. The figure shows that the amplitude of the axial oscillations is limited to about 1.5 cm. Charge state Q, kinetic energy E and energy loss $\delta E/\delta s$ of a single 610 MeV ion are shown in Figs. 5 and 6 as a function of the travelled path s. In Fig. 7 the kinetic energy of the ions is plotted as a function of
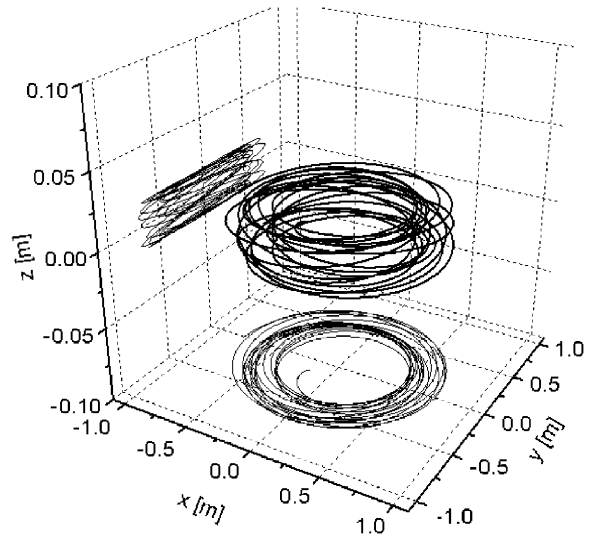

Fig. 2. 3D trajectory of a ^{78}Br ion injected with $E = 610$ MeV into a weakly focusing magnetic field with a maximum field strength of $B = 2$ T. A helium pressure of 10 mbar is used.
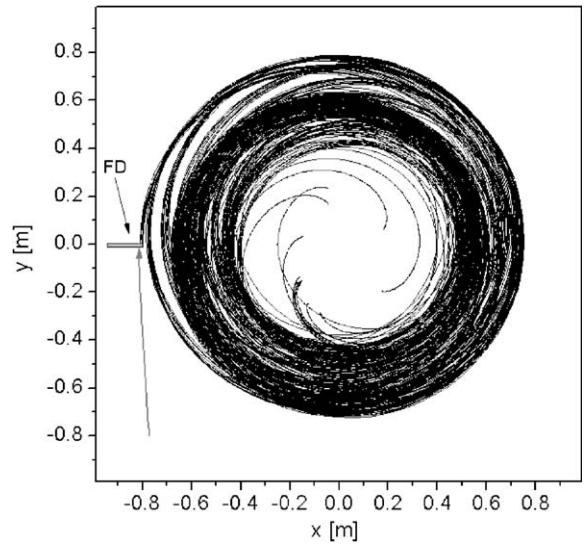

Fig. 3. Trajectories projected onto the x–y plane of ions having passed a solid degrader (FD). Energies of 550–670 MeV and different start positions and angles as indicated in Table 1 have been used for the trajectory calculations.

their radial distance from the magnet center. It indicates that the major energy loss happens at radii much larger and clearly separated from those
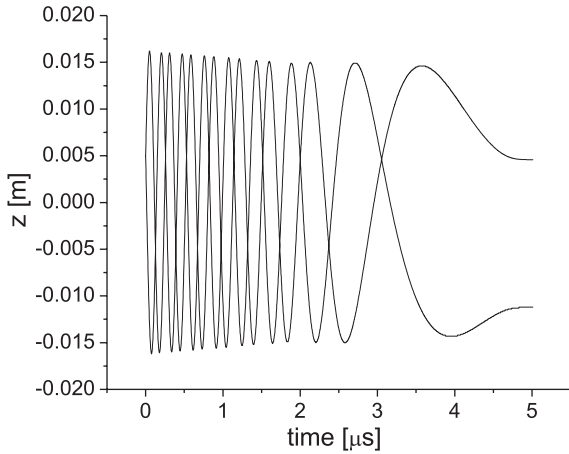
Fig. 4. Vertical position z of two test ions as a function of time during the slowing down process.
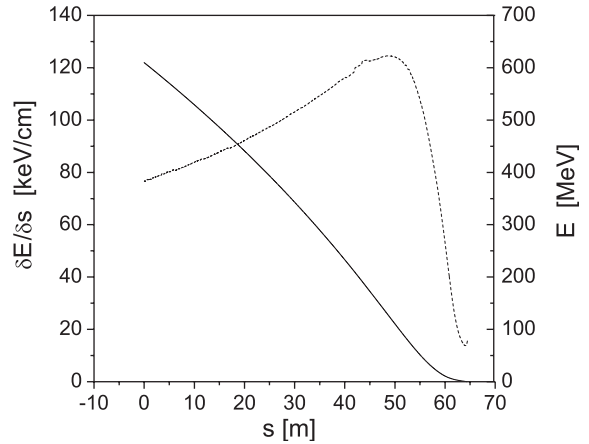

Fig. 6. Energy loss $\delta E/\delta s$ (dashed line) and energy E (solid line) of a stopping ion as a function of path length s.
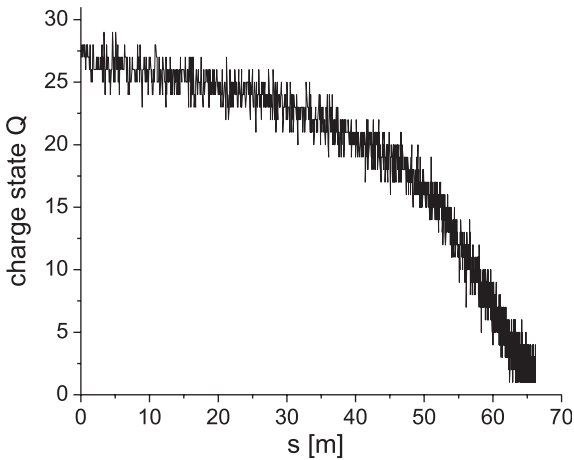

Fig. 5. Charge state Q of a stopping ion as a function of path length s.
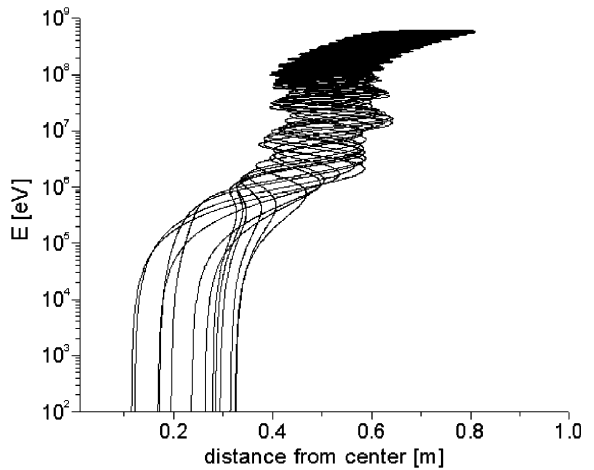

Fig. 7. Energy E versus distance r of the ions from the magnet center of the proposed system.

at which the ions finally stop. The typical flight time of a 610 MeV ion in the present system is about 5 μs. The total flight path is about 65 m, which (not too surprisingly) is in good agreement with a range of 63 m predicted by SRIM for these ions.

For the practical purpose of collecting fast ions stopped in gas the final ion distribution and the energy loss (ionization) in the gas are important. The final ion distributions for 10,000 ions with random beam properties within the parameter

space given in Table 1 are shown in Figs. 8 and 9. The distributions are toroidal with an outer radius of less than 30 cm and a height of less than 3 cm. This means that the ions are collected in a well defined volume, which is essential for their efficient extraction and transformation into a low-energy ion beam.

Fig. 10 shows the integrated energy deposition of 10,000 ions in the x–y plane as a 2D grey-scale plot. The remarkable feature of the proposed system is that the energy deposition in the gas and
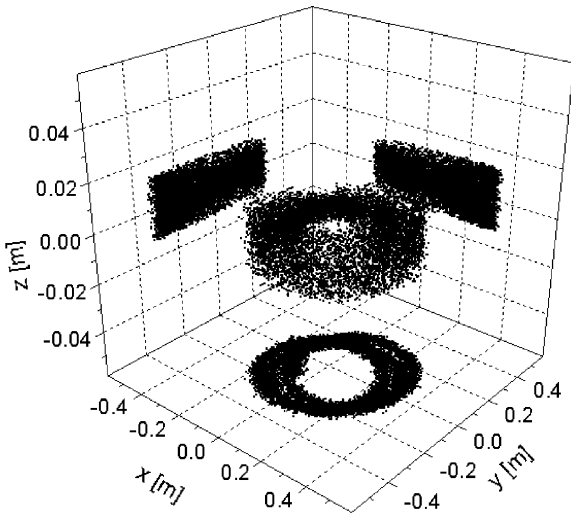
Fig. 8. Final distribution in space of ions with kinetic energies of less than 100 eV.
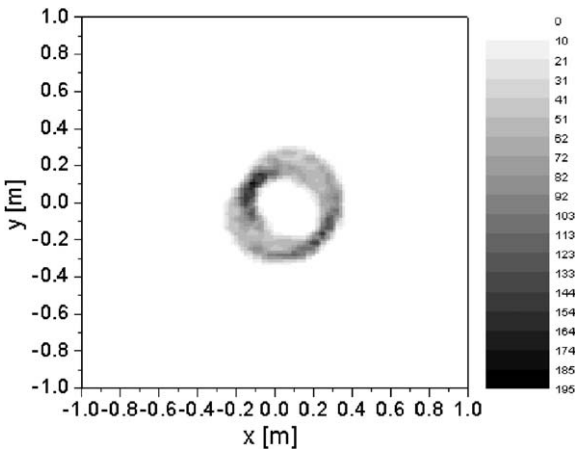

Fig. 9. Ion density in x–y plane for 10,000 ions (grey scale coding unit is ions/$(16\,cm^2)$).

Fig. 10. Total energy deposition in x–y plane for 10,000 ions (grey scale coding unit is keV/$(16\,cm^2)$).

the corresponding level of ionization has a maximum well outside the area where the ions finally stop (see Fig. 9). This means that space charge effects in this extraction zone, if any, will be solely due to the stopped ions and not be enhanced by the helium ionized during the stopping process. The peak energy loss observed for all 10,000 ions is 1.9×10^7 keV in an integration area of $4\,cm \times 4\,cm$. The average energy loss within the torus of main ionization is less than half of this value.

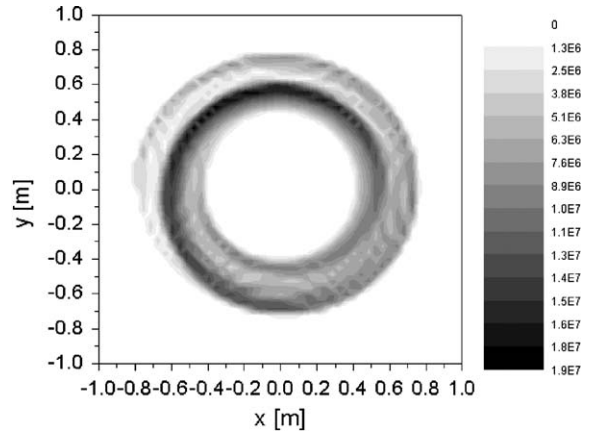Taking a thickness of the stopping volume of 3 cm (see Fig. 4), the maximum energy loss created per ion in a volume of $1\,cm^3$ is about 40 keV. With an energy of about 41 eV required to ionize helium, the maximum number C_i of helium ions created per incident bromine ion in such a volume is less than 1000.

Additional simulations have been performed for ^{40}Ca and ^{120}Sn ions in order to evaluate if the scheme can be applied to a larger mass range. For this simulations the same beam parameters as for bromine (Table 1) were used and only the helium pressure and the magnetic field strength were adjusted. Fig. 11 shows energy loss and final density distributions for both ion species. As for the bromine case one observes a good separation between the region of high ionization and that where the ions come to rest.

3.1.3. Evaluation of space charge limits

The proposed scheme provides the possibility to very effectively collect the charges produced by the ionization of the helium gas. Electrodes in the top and the bottom of the chamber as indicated in Fig. 1 can be used to produce a weak electric field in the direction of the magnetic field. We assume a field strength of $E = 3000$ V/m. For a few-centimeter gap the potential difference is kept well below the breakthrough voltage for helium of about 150–200 V in this pressure regime [21]. The reduced ion mobility k_0 for He$^+$ in He at room
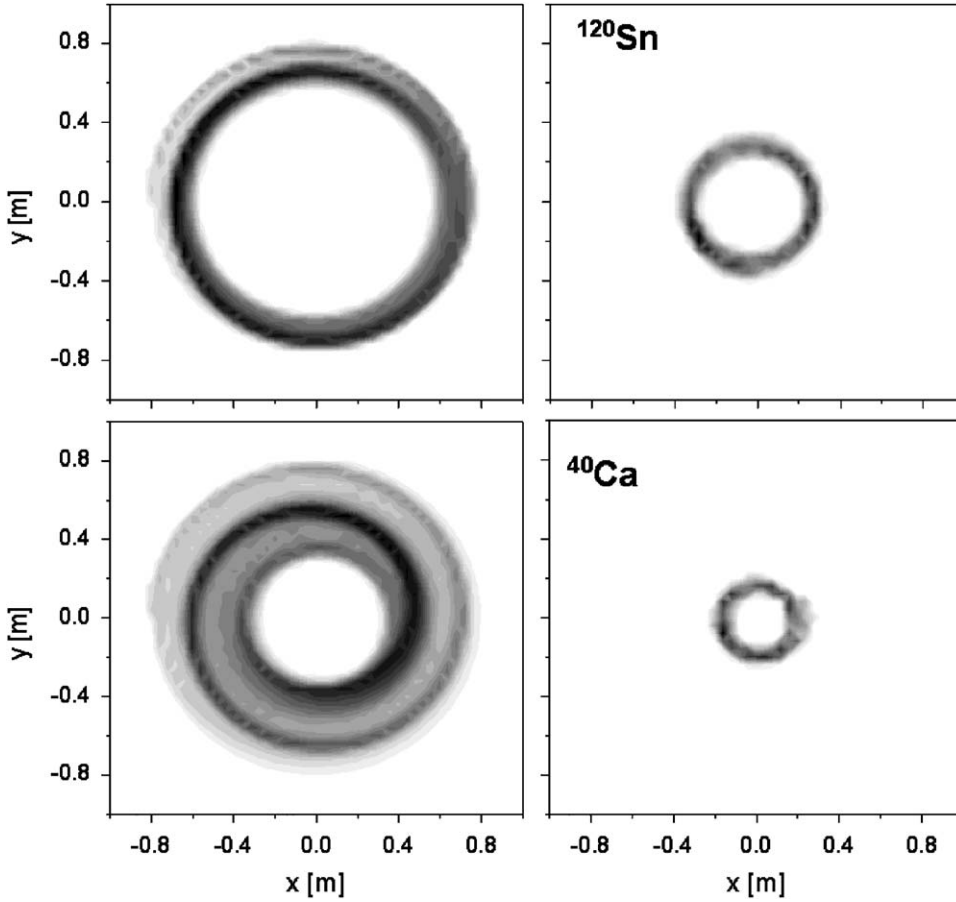
Fig. 11. Energy deposition during stopping process (left) and density of stopped ions (right) for 610 MeV Sn (top) and Ca ions (bottom). $B = 2.1$ T and $p_{He} = 6$ mbar was used for Sn and $B = 1.9$ T and $p_{He} = 25$ mbar for Ca.

temperature is about $k_0(He) = 1.05 \times 10^{-3}$ m^2/ (Vs) for low drift velocities [22]. For a pressure of $p_{He} = 10$ mbar and the assumed electric field strength this results in a He$^+$ drift velocity of $v_d = k_0(He) \cdot (1024 \text{ mbar})/p_{He} \cdot E \approx 300$ m/s.

In order to remove the helium ions from the stopping volume they have to travel a maximum distance of the thickness of the cloud, i.e. 3 cm (see Fig. 4). With the given drift velocity v_d this is achieved in about 1×10^{-4} s. Since the mobility of the electrons is much higher they do not need to be considered in first order.

Huyse et al. [23] have analyzed space charge limits in gas stoppers using results obtained for drift chambers. In contrast to "conventional" gas stopper systems the proposed system resembles

very closely a classical parallel-plate drift chamber. Considerations for such a system should therefore be well applicable. The incident heavy ion creates pairs of helium ions and electrons. While the electrons are removed quickly by the electric field the slower He ions move towards the cathode and induce a voltage [24]

$$V_{\text{ind}} = \sqrt{\frac{eQ}{4\varepsilon_0 k}} d^2. \tag{6}$$

Here e is the electron charge, ε_0 is the electronic constant, Q is the ionization rate per volume, d is the distance between the plates, and $k = k_0(He) \cdot (1024 \text{ mbar})/p_{He}$ is the mobility of the helium ions at the given pressure p_{He}. The charge collection

process will saturate when the net field between the plates is reduced to zero. This is the case when V_{ind} equals the applied voltage V_{appl}. From Eq. (6) the maximum rate Q_{max} can be calculated. For a separation of $d = 4$ cm between the two collection plates, an electric field strength of $E = 3000$ V/m and a helium pressure of $p_{He} = 10$ mbar we obtain $Q_{max} = 1.3 \times 10^{11}$ ion–electron-pairs/s/cm^3. In order to reach such an ionization rate a beam rate of at least $R = 10^8$/s is required if we assume $C_i = 1000$ as obtained from the simulations.

These estimates indicate that the proposed system will be able to handle beam rates more than four orders of magnitude larger than the rate values for which efficiency losses in "conventional" gas stopping systems for high-energy (> 50 MeV/u) beams have been reported [1,4]. The rate of $R = 10^8$/s is a very conservative limit and the maximum tolerable beam rates are expected to be significantly larger. The reason is that space charge will not affect the ion trajectories as long as the beam energy is large compared to all induced and applied voltages. As already discussed, this is the case in the region of highest ionization. The ionization rate is low in the volume where the ions finally stop and from where they are extracted.

3.2. Ion injection

In the present scheme it is foreseen to have the ions first pass a set of adjustable solid degraders before they enter the stopping chamber through a thin entrance window. A final solid degrader reduces the beam energy further to bring the ions onto the desired injection trajectory. Ion injection into the stopping chamber has to be done such that the ions do not hit the final degrader again after one turn in the magnetic field. If the beam parameters (energy spread, transverse emittance) are similar to those listed in Table 1, there will be a clear separation between the edge of the final degrader and the ion trajectories after one turn. For the case shown in Fig. 3 the distance between the trajectories and the edge of the degrader is more than 1 cm. The calculations performed in this work also indicate that for achieving the maximum separation between final degrader and first turn it

is best to use an injection radius that corresponds to the high-energy end of the energy distribution of the beam. For the results shown here an injection radius of $r_{inj} = 0.8$ m was chosen that corresponds to an injection energy of $E_0 + \Delta E = 670$ MeV.

The beam properties listed in Table 1 are conservative in terms of achievable beam size, emittance and energy spread of secondary beams from present fragmentation facilities. They fully cover the properties of secondary, energy degraded beams available at the NSCL. However, the proposed scheme should be able to accommodate beams with even less favorable properties than those used here. There are a number of additional means to minimize injection losses resulting from trajectories that come too close to the final degrader channel. One possibility is to use momentum compression in such a way that the dispersion plane is parallel to the magnetic field used here. In this way a small beam spot size in the critical radial direction can be realized. The larger beam size in the dispersion direction can be tolerated as long as the beam size is smaller than the height of the vacuum chamber. Other scenarios to avoid beam losses at the final degrader are to deliberately introduce vertical or betatron oscillations tailored to avoid the degrader during their first turn. Still to be studied in more detail, it may also be possible to install thin foil degraders along the circumference of the first turn in such a way that ions travelling at too large orbits will suffer an increased energy loss and move towards the center.

3.3. Ion extraction

The final ion distributions shown in Figs. 8 and 9 indicate that the most favorable direction to extract the ions is through an axial opening in the magnet system. A technique is needed for guiding the ions to such a bore and for transporting them through a differential pumping system before the beams can be accelerated and a low-energy beam can be formed.

The extraction of the ions from gas cells operated at low pressure is best done with radio-frequency funnels [18,25] or carpets [4,17]. As already proposed in Ref. [17], an RF carpet is the best choice for collecting and transporting of the

ions stopped in the toroidal volume shown in Fig. 8. RF carpets are based on a series of narrow and narrow-spaced concentric electrodes to which RF voltages are applied such that neighboring electrodes have opposite phase. For proper amplitudes and frequencies such an RF carpet provides a repulsive potential to an ion approaching it. Additional static voltages can be applied to create an electric field that guides the ions towards a central hole. Thus, ion funnels and subsequent RF ion guides can be used to transport the ions through the magnet bore. A possible complication in the discussed scheme is the presence of the strong and changing magnetic field and its effect on the ion transport properties of RF based devices.

3.3.1. Simulation of the effect of a magnetic field on RF ion guiding

We have used SIMION [26] to simulate the effect of a 2-Tesla magnetic field on the performance of an RF carpet. The carpet geometry and fields have not been carefully optimized since the purpose of these simulations is to only reveal major obstacles in using such a scheme. Fig. 12 shows parts of the geometry used in the RF carpet simulation. The spacing between the different rings is 1 mm and the disks are 0.5 mm wide. The carpet is operated with an RF amplitude and frequency of 400 V and 1.5 MHz, respectively. The radial electric field gradient over the carpet surface is about 20 V/cm and increases to > 100 V/cm inside the funnel-like central part. An electrode (not shown in the figure) placed at a distance of 2 cm parallel to the carpet surface is used to provide an electric field component in the direction of the carpet. Singly charged ions with $A = 78$ are used in the trajectory simulation. The simulations show that the ions are safely guided along a height of more than one millimeter from the carpet electrodes. The main effect of the magnetic field is to introduce a slight curvature into the drift motion along the carpet surface and the overall ion guiding characteristics of this RF device are
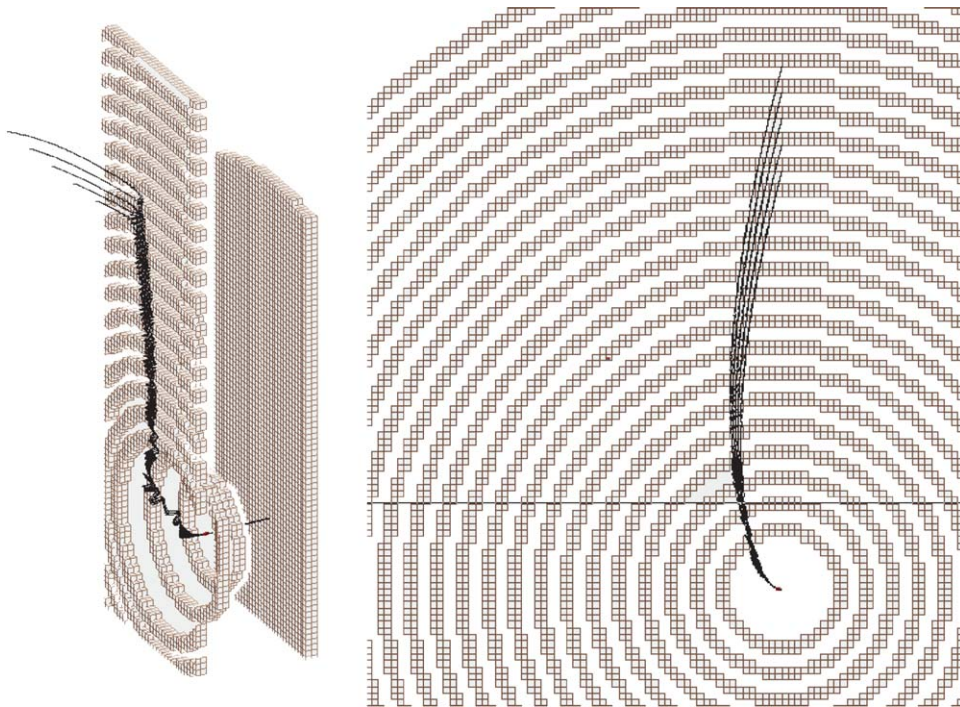

Fig. 12. SIMION calculation for an ion approaching an radiofrequency carpet with a 2-Tesla magnetic field perpendicular to its surface. Left: 3D sectional view. Right: top view.

practically not affected. The extraction time of an ion from the starting point at a radius of about 1.5 cm through the central funnel is less than 50 µs. For a larger carpet with a 40 cm radius it should be possible to achieve similar drift velocities. This means that ion transport times from the rim of the carpet to its center of less than two millisecond are realistic.

3.3.2. Estimated total ion extraction time

For the transport of the ions collected inside the toroid shown in Fig. 8, we assume an average electric field component pointing towards the carpet with a strength of 500 V/m and a total path of 4 cm to be travelled to reach the pseudo potential wall provided by the carpet. Using a typical value for the ion mobility $k_0 = 2 \times 10^{-3}$ m^2/(Vs) for heavy ions in helium and a pressure of 10 mbar results in a drift velocity of 100 m/s and a transport time for this distance of 0.5 ms. Together with the stopping time, the extraction time along the carpet surface through the funnel, and transport in a linear RFQ ion guide to a point outside of the magnet a total extraction time below 5 ms can be achieved for all ions. This value matches well the half-life of the shortest-lived isotopes and is at least an order of magnitude shorter than that of "conventional" gas stopping systems.

4. Conclusions

A scheme for the efficient thermalization of energetic and intense rare isotope beams has been studied using simulations and calculations. The results indicate that gas stopping in a weakly focusing magnetic field has the potential to overcome the severe intensity limitation that exist in present systems and to provide a faster ion extraction. The results obtained for the slowing down, the collection of ionization, and the extraction of the ions reveal that there are major advantages of this scheme over previous approaches. In summary, they are

- Efficient stopping of beams with energies of 100 MeV/u at rates of 10^8/s and possibly

higher, rates that are expected at next-generation rare isotope beam facilities.
- Extraction times of less than 5 ms that avoid decay losses and match the benefits of fast beam production.
- Short extraction times and low gas pressure that minimize possible effects from ion chemistry and charge exchange.
- A large beam acceptance that allows for faster incident beam tuning.

More studies are still required before an optimized system can be built. Systematic investigations have already started for systems using different magnetic field strengths and field indices, as well as for different gas pressures. It can already be concluded that there is a wide range of parameters that can be used. For example, larger magnetic fields have the advantage of smaller injection radii and stopped-ion distributions with smaller diameter but require higher gas pressures to achieve enough turn separation. Additional simulations will also be required for the ion injection into the system, for the study of advantage or disadvantage of distributed degrader schemes or of a varying field index, and for the optimization of the ion extraction.

References

[1] L. Weissman, et al., Nucl. Instr. and Meth. A 540 (2005) 245.
[2] G. Sikler, et al., Nucl. Instr. and Meth. B 204 (2003) 482.
[3] G. Savard, et al., Nucl. Instr. and Meth. B 204 (2003) 582.
[4] M. Wada, et al., Nucl. Instr. and Meth. B 204 (2003) 570.
[5] B.M. Sherrill, Nucl. Instr. and Meth. B 204 (2003) 765.
[6] G. Savard, Nucl. Instr. and Meth. B 204 (2003) 771.
[7] H. Geissel, et al., Nucl. Instr. and Meth. A 282 (1989) 247.
[8] H. Weick, et al., Nucl. Instr. and Meth. B 164–165 (2000) 168.
[9] C. Scheidenberger, et al., Nucl. Instr. and Meth. B 204 (2003) 119.
[10] L. Weissman, et al., Nucl. Instr. and Meth. A 522 (2004) 212.
[11] L. Weissman, et al., Nucl. Instr. and Meth. A 531 (2004) 416.
[12] L. Weissman, et al., Nucl. Phys. A 746 (2004) 655c.
[13] M. Wada, private communication (publication in preparation).
[14] S. Schwarz, publication in preparation.
[15] L.M. Simons, Phys. Scripta T22 (1988) 90.

[16] L.M. Simons, Hyperfine Interactions 81 (1993) 253.
[17] I. Katayama, et al., Hyperfine Interactions 115 (1998) 165.
[18] S. Masuda, et al., in: Advances in Static Electricity, Auxillia Brussels, 1970, p. 398.
[19] J.F. Ziegler, SRIM-2003, http://www.srim.org/srim
[20] H.D. Betz, Rev. Mod. Phys. 44 (1972) 465.
[21] P. Hartmann, et al., Plasma Sources Sci. Technol. 9 (2000) 183.
[22] A.S. Dickinson, et al., J. Phys. B. 32 (1999) 4919.
[23] M. Huyse, et al., Nucl. Instr. and Meth. B 187 (2002) 535.
[24] J. Sharpe, Nuclear Radiation Detectors, Methuen, London, 1964.
[25] T. Kim, et al., Anal. Chem. 72 (2000) 2247.
[26] D. Dahl, Int. J. Mass Spectrom 200 (2000) 3.